Shear wave velocity update using PS reflection FWI for imaging beneath complex gas clouds

M. Wang[1], Y. Xie[1], P. Deng[1], J. H. Tan[1], S. Maitra[1], M. Camm[2], N F. S Zaina[2], W. H. Tang[3], M N. B M Isa[3], A A. B Muhamad[3]*
[1] CGG, [2] KPOC, [3] PETRONAS

Summary

Shear wave (S-wave) velocity model building (VMB) is a critical and difficult step in converted-wave imaging (PS imaging). Conventional S-wave VMB depends on PP-PS joint interpretation-based image registration and PP-PS joint tomography-based residual moveout (RMO) flattening. Recently, the advent of multi-modal surface wave inversion (SWI) addressed some of these issues by resolving near-surface S-wave velocity (V_s) variations that cause large static effects (~100 milliseconds). However, all of the processes listed above have certain advantages and drawbacks.

We describe a PS reflection full-waveform inversion (PS-RFWI) for S-wave VMB in the presence of a complex, heterogeneous subsurface that can address some of the concerns with conventional approaches. This method assumes that we have already obtained sufficiently accurate pressure wave (P-wave) velocities and reflectivity. PS-RFWI solely updates V_s by minimizing the kinematic difference between the modeled and recorded PS reflections, while leaving the P-wave parameters unchanged. In conjunction with conventional methods, PS-RFWI can provide a superior PS image, as we demonstrate with a field data example from offshore Malaysia.

Introduction

Historically, the seismic industry has understood the promise of PS or S-wave data. However, only in the past decade have advances in acquisition and processing technology, along with compute capacity, made it possible to realize the potential of PS imaging. Mainly seen as a tool to provide complementary information in areas where the P-wave (or PP) image is affected by complex shallow gas clouds (Akalin et al., 2014; Yusoff et al., 2015), PS imaging can additionally identify different types and qualities of reservoirs (Stewart et al., 2003). This is because, unlike P-waves, S-waves are not affected by pore fluid saturation, and instead are only affected by compaction or lithology.

Building accurate S-wave model parameters is critical for successful PS depth migrations; however, this has remained one of the main challenges in unlocking the full potential of PS imaging. At present, the conventional tools for S-wave VMB include SWI, PP-PS event registration, and PP-PS joint tomography. SWI can provide a high spatial-resolution V_s model in the near surface (Li et al., 2019) by making use of surface waves that propagate horizontally along the near surface. However, SWI's effectiveness is limited to 100-200 meters beneath the water bottom due to the exponential decrease of surface-wave energy with increasing distance from the water bottom interface. PP-PS event registration is a commonly used approach and can, in theory, provide velocity updates from shallow to deep depths. This method relies on the principle that PP and PS waves, for the same subsurface reflector, should migrate to the same depth. Therefore, depth errors between PP and PS images are measured event-by-event, which in turn are used to update the V_s model based on either a 1D ray path assumption or more sophisticated 3D map migrations (Birkeland et al., 2014). The effectiveness of these approaches can vary due to a few practical challenges: poor PS events at shallow depths due to sparse ocean bottom seismic (OBS) acquisitions; ambiguity of PP and PS event correspondence due to large velocity errors; and different seismic characteristics of the PP/PS pair in reflectivity, frequency, bandwidth, and phase, resulting from natural PP/PS wave propagation and processing. In cases of complex structures, ray-based 1D or 3D map migrations may also fail to provide adequate S-wave velocity updates. Joint PP-PS reflection tomography, as an approach extended from conventional P-wave tomography, focuses on reducing RMO errors by perturbing one or more model parameters using RMO picks from PP and PS common image gathers (CIGs) simultaneously. The challenge for PP-PS tomography is usually due to poor quality PS CIGs as a result of uneven PS angle illumination from sparse OBS surveys that are typically designed for optimizing PP data. In addition, PP-PS tomography shares similar limitations as PP tomography for a single-arrival ray-based approach.

Full-waveform inversion (FWI) has established itself as an important tool for building an accurate pressure wave velocity (V_p) model. Naturally, FWI with full elastic modeling should be the desired solution for PS VMB. While elastic FWI is an active research area, it is still a long way from becoming a common tool for PS imaging due to the associated algorithm complexity and computational cost.

Our approach was inspired by the learnings from developing acoustic FWI to robustly derive high-resolution P-wave velocity, including decoupling kinematics and amplitudes and extracting the low-wavenumber tomographic term of the FWI gradient for reflection updates. We propose a new practical and affordable FWI algorithm for updating the V_s model using PS reflection energy. With this process, we update V_s after P-wave velocity analysis using P-waves, while keeping V_p, anisotropy, and attenuation (Q) fixed

(Masmoudi et al., personal communication, 2021). A cross-correlation weighted time-lag cost function is used to further stabilize the inversion against the discrepancy between PP and PS reflectivity. When compared with conventional approaches, PS-RFWI, as a data-driven approach, has obvious advantages, such as honoring 3D wave propagation, handling complex structures, and hence providing more accurate spatial variations in velocity. In the following sections, we describe our PS-RFWI and demonstrate its benefits in improving the reservoir image underneath complex gas clouds with a field OBS data set.

Method

PS reflection data are generated by mode conversions at sharp model interfaces, which can be highly elastic in nature. However, given that modern practices are more established with acoustic FWI than elastic FWI, we decouple this elastic process into separate P-side acoustic wave propagation using V_p, and S-side acoustic wave propagation using V_s. We adopt P-wave Born modeling as proposed by Xu et al. (2012) to simulate the PS reflection energy. Three model parameters are needed to describe the Born approximation of PS data: a smooth background P-wave velocity model (V_{p0}), a background S-wave velocity model (V_{s0}), and a high-wavenumber S-wave perturbation (δm). First, we assume there is an incident P-wave (P_0) propagating in the background model, taking the isotropic case as an example:

$$\frac{1}{V_{p0}^2}\frac{\partial^2}{\partial t^2}P_0 = \nabla^2 P_0 + F\,, \qquad (1)$$

where F is the source term. If this incident wavefield encounters a high-wavenumber S-wave perturbation, a secondary source is excited and a scattered S-wave (S) is generated that propagates in the background model (V_{s0}) as:

$$\frac{1}{V_{s0}^2}\frac{\partial^2}{\partial t^2}S = \nabla^2 S + P_0(\boldsymbol{x},t)\delta m(\boldsymbol{x})\,, \qquad (2)$$

where the second term on the right-hand side of Equation 2 is the secondary source.

In practice, we use a P-wave reflectivity model as the high-wavenumber S-wave perturbation in Equation 2 instead of S-wave reflectivity, even though they are often quite different (Stewart et al., 2003). This choice is made with a rationale similar to that used in conventional PS imaging. Since P-wave VMB and imaging techniques are better established than S-wave VMB, it is reasonable to assume the PP image/model are accurate, and hence fixed, and to adjust the PS image/model to be kinematically consistent with its PP counterparts. Ideally, we want to update both the P-wave image/model and S-wave image/model simultaneously. However, too many degrees of freedom make this highly nonlinear process unstable. By fixing the P-wave image and velocity and replacing the S-wave reflectivity with P-wave reflectivity, PS-RFWI becomes more tractable. This allows the inversion of only one parameter, i.e., S-wave velocity, while freezing the P-wave velocity and all other anisotropy parameters. The corresponding low-wavenumber gradient of the S-wave velocity can be derived from the above equations (Masmoudi et al., personal communication, 2021).

The acoustic demigration process in Equations 1 and 2 produces correct kinematics of PS reflections, even though the amplitude behavior relative to the observed data is different. In this proposed PS-RFWI methodology, we use the traveltime difference ($\Delta\tau$) between the modeled PS reflection data and the recorded PS reflection data as the cost function to stabilize the inversion process by downplaying the amplitude effects. The time shift is measured by a dynamic warping approach, which employs a global search with constraints (Hale, 2013). The cost function for PS-RFWI can be described as:

$$J_{TT}(m_0,\delta m) = \|\Delta\tau(\delta d, \delta d_{calc}(m_0,\delta m))\|_2^2\,, \qquad (3)$$

where δd represents the recorded PS data and $\delta d_{calc}(m_0,\delta m)$ is the modeled PS data. Cycle-skipping is a well-known challenge for FWI since it is a local inversion process. It can be an issue for PS-RFWI as well, due to uncertainties in the initial S-wave velocity model. This issue is partially mitigated by the cost function in Equation 3, which has a better convexity and is less sensitive to amplitude discrepancy when compared to the standard least-squares cost function.

As discussed, we use PP reflectivity rather than PS reflectivity as the high-wavenumber perturbation δm for generating PS reflections in Equation 2. In reality, there exist differences between PP and PS reflectivity due to different seismic responses to changes in V_p, V_s, and density terms. This can also pose difficulties in time-lag measurements. To counter this, we make use of the cross-correlation between the modeled and observed PS data with a weighting factor w_c applied for more appropriate data matching (Zhang et al., 2018). Therefore, the cost function can be updated as:

$$J_{TTW}(m_0,\delta m) = \|w_c\Delta\tau(\delta d, \delta d_{calc}(m_0,\delta m))\|_2^2\,. \qquad (4)$$

The weighting factor w_c helps improve the robustness of the inversion against reflectivity differences and noise in the recorded PS data by promoting reliable high-quality measurements, while suppressing poorer quality data.

Application

We applied PS-RFWI on a 3D 4C ocean bottom node data set from Offshore Sabah, East Malaysia. The data was acquired with 300×300 m node spacing for most of the survey and 150×150 m node spacing for the area above the gas body, as shown in Figure 1. The shot spacing is 50 m, with a maximum offset of 16 km. The water depth ranges from 200 m to 800 m, while the target, highlighted with a dashed yellow polygon in Figure 2, is at the top of an

anticlinal thrust just underneath the slow, gas-filled slump body. With robust Time-lag FWI (Zhang et al., 2018) for P-waves, we ran a joint V_p and Q inversion to produce high-resolution V_p and Q models (Tan et al., 2021). PP imaging with Q compensation provided a reasonable image at the reservoir level; however, we observe that the top of the reservoir is not clear in the PP image (Figure 2c). Furthermore, the internal bedding of the thrust-fold structure has low resolution due to strong absorption in the overburden. The PS image has the potential to provide complementary information due to the different responses through the gas clouds when compared with the PP image. Therefore, 4C data was acquired to look for possible uplift from the PS image. SWI was unable to update Vs in the complex gas clouds, as these were below the penetration depth of the surface waves. Conventional PP-PS registration was performed first, but it was unable to reliably update V_s inside and below the gas zone. One of the reasons is the poor quality of the PS image from the sparse node sampling; the swing and the discontinuity of reflectors can be observed in the shallow section of Figure 2a. The PS image shown in Figure 2a was obtained using an S-wave velocity model after conventional PP-PS registration. We observe that the structures inside the reservoir are not well imaged, and the PS events are not well aligned with the PP events due to unresolved V_s variations in the overburden.

PS-RFWI was performed on the PS reflection data using the above mentioned S-wave velocity model as the initial model (Figure 3a). The PP image was supplied as the reflectivity model to generate PS reflections and update the S-wave velocity by minimizing the traveltime difference between the synthetic and the observed PS data. Rich low-frequency signal from the OBS acquisition helped mitigate the cycle-skipping problem. We performed PS-RFWI from 3.5 Hz to 4.5 Hz using data with a maximum offset of 6 km. The updated S-wave velocity model, shown in Figure 3b, better correlates with the geology. The resultant PS image shown in Figure 2b has well-imaged PS events that are better aligned with the PP events from Figure 2c. At the same time, it gives a clearer image for the top of the reservoir, as well as improved internal bedding structures inside the reservoir interval. The gas-oil contact (GOC, dashed blue line in Figure 2c) appears as a staggered flat spot and can be observed on the PP image because pressure waves are sensitive to fluid saturation, while it is not visible on the PS image since converted waves are insensitive to changes in fluid content. Such comparisons of PP and PS reflectivity can help identify fluid contacts and improve structural interpretation. Figure 4 shows a migrated stack section using the S-wave velocity model after PS-RFWI, together with comparison of CIGs before and after PS-RFWI update. CIGs using the PS-RFWI velocity model are clearly flatter and more focused than the ones before the V_s update, giving us confidence in the update.

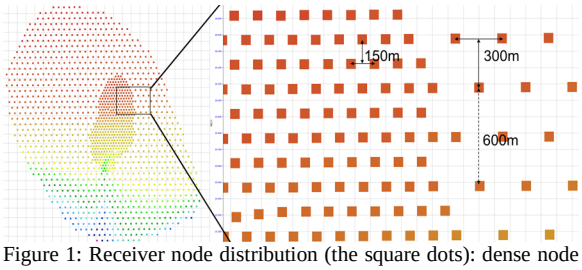

Figure 1: Receiver node distribution (the square dots): dense node sampling above gas area, with coarse node sampling elsewhere.

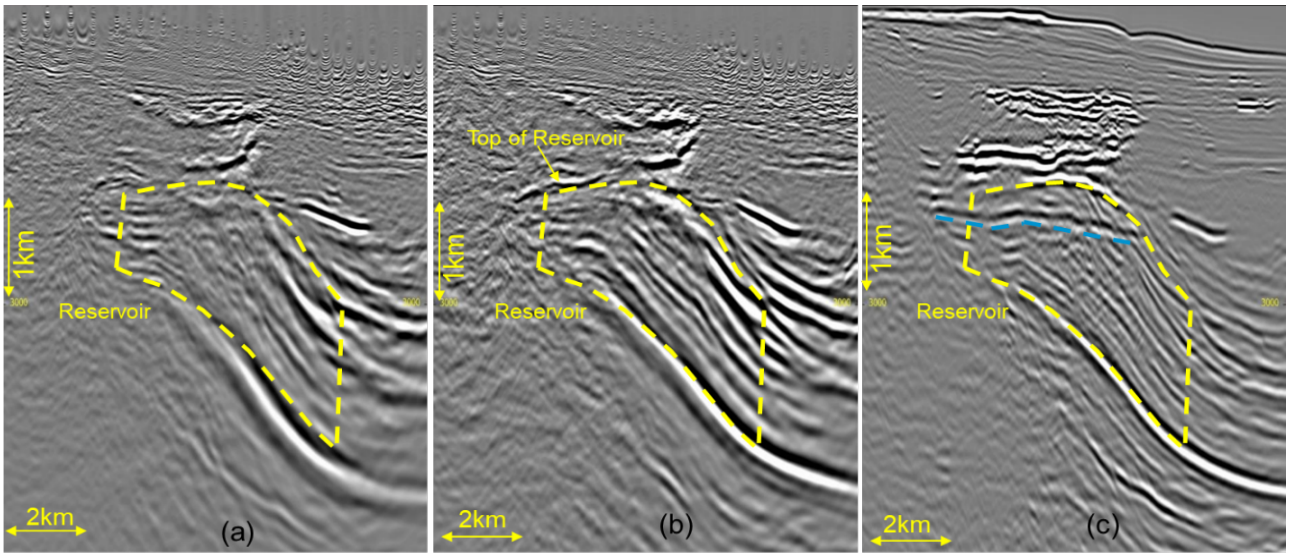

Figure 2: (a) PS-QRTM image before PS-RFWI. (b) PS-QRTM image after PS-RFWI. (c) PP-QRTM. The reservoir has been highlighted.

Discussion

Our choice of fixing the P-wave velocity and image and replacing the S-wave reflectivity by the P-wave reflectivity may contain considerable errors, since the S-wave reflectivity can be different from the P-wave reflectivity. To enable the update of the S-wave velocity for this data set, it was important to stabilize the inversion. In addition to stabilizing the inversion through reduced degrees of freedoms/non-linearity, we found that our strategy also stabilizes the inversion through mitigating the depth-velocity ambiguity issue typically encountered in conventional P-wave RFWI, where both reflectivity and velocity are unknown variables for inversion. The ambiguity between S-wave reflectivity and velocity is even larger because V_s is often much slower. If we allow both the P-wave image and velocity and the S-wave image and velocity to change, the large ambiguity from both the P-side and S-side can similarly make the inversion unstable. In our strategy, we acknowledge that V_p errors could possibly leak into the V_s model update, but considering the longer traveltime on the S-leg due to the slower S-wave velocity, the PS imaging will be less sensitive to V_p errors than V_s.

The fundamental limitation of this adjoint-state based approach is the local minimum inversion. The success of FWI relies on good data quality and a robust inversion approach. When the data quality is sub-optimal, the starting point for the inversion becomes more important so as not to suffer from cycle-skipping. Therefore, we still have to rely on the conventional approaches of SWI, PP-PS registration, and PP-PS joint tomography to derive a good initial V_s model. These, in conjunction with the cost function in Equation 4, help reduce issues arising from cycle-skipping. Furthermore, taking partial stacks as reflectivity models for Born modeling, as discussed by Wang et al. (2018), would be a good way to further reduce the possibility of cycle-skipping.

Vertical resolution is another challenge for PS-RFWI due to the small incidence angle coverage of PS reflection energy. Optimal angular distribution of reflections and visible reflection energy at different depths are needed for the success of PS-RFWI. Some strategies like weak reflectivity enhancement, layer-stripping schemes, and structurally constrained smoothing would help to a certain extent.

Keeping all of these factors in mind, we estimate that the effectiveness of the PS-RFWI approach will be data and workflow dependent, but can be a powerful tool if the right conditions exist.

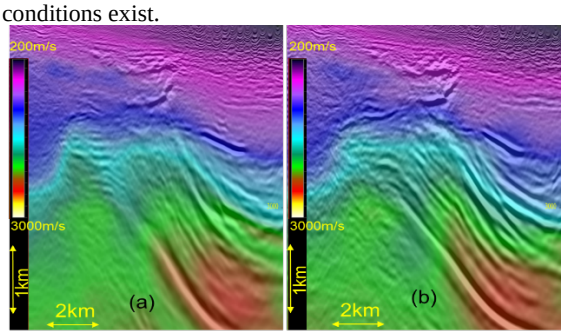

Figure 3: V_s model (a) before PS-RFWI and (b) after PS-RFWI.

Conclusions

We proposed a workflow to update the S-wave velocity model using PS-RFWI. This approach addresses some drawbacks of conventional S-wave VMB methods in the presence of complex structures by honoring 3D wave propagation. PS-RFWI captures lateral variations in the S-wave velocity field, resulting in an improved PS image. This PS image provides complementary information, and when used in conjunction with the PP image, can help reduce the uncertainty and risk in the discovery or development of hydrocarbon reservoirs.

Acknowledgments

The authors thank CGG, KPOC, and PETRONAS for permission to publish this work and KPOC for permission to show the data examples. We also thank Tengfei Wang for his contributions in early development and Nikk Johari Low for the processing of this data. Special thanks to Qing Xu and Ping Wang for the paper review and fruitful discussions.

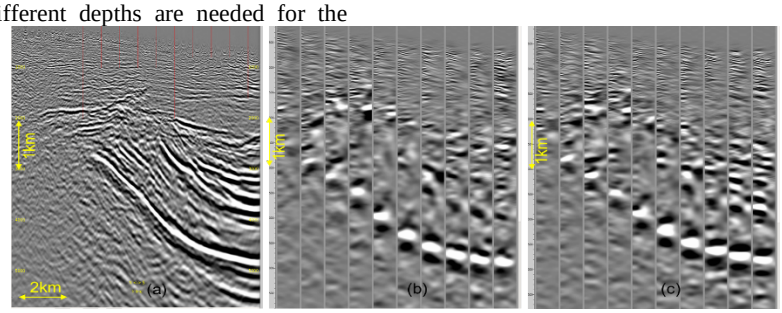

Figure 4: (a) PS-Q-Kirchhoff migration stack using V_s after PS-RFWI. PS image gathers using V_s (b) before and (c) after PS-RFWI. The maximum offset shown here is 8000 m.

References

Akalin, M. F., A. A. Muhamad, Y. C. Tan, Y. B. M. Yusoff, N. A. M. Radzi, S. F. M. Zohdi, M. H. Hashim, M. Ghazali, S. Maitra, A. Wardoyo, M. L. Ghazali, J. V. S. Murthy, G. Wang, and X. G. Miao, 2014, 3D-PS converted waves solving 3D-imaging challenges under gas clouds – Offshore Malaysia: 76th Conference and Exhibition, EAGE, Extended Abstracts, Tu D202 03, doi: https://doi.org/10.3997/2214-4609.20140639.

Birkeland, O. J., P. Guillaume, T. Krishnasamy, L. D'Afonseca, T. M. G. Santiago, and C. Guerra, 2014, Tomographic co-depthing of PP and PS horizons by S-Ray approximation: 84th Annual International Meeting, SEG, Expanded Abstracts, 1837–1841, doi: https://doi.org/10.1190/segam2014-0806.1.

Hale, D., 2013, Dynamic warping of seismic images: Geophysics, **78**, no. 2, S105–S115, doi: https://doi.org/10.1190/geo2012-0327.1.

Li, X., Y. Chen, X. Miao, L. Li, F. C. Loh, B. Hung, S. Wolfarth, and D. Priyambodo, 2019, High resolution multi-model surface wave inversion for shallow S-wave velocity model building: 81st Conference and Exhibition, EAGE, Extended Abstracts, Tu R09 07.

Stewart, R., J. Gaiser, R. Brown, and D. Lawton, 2003, Converted-wave seismic exploration: Applications: Geophysics, **68**, no. 1, 40–57, doi: https://doi.org/10.1190/1.1543193.

Tan, J. H., M. Z. Jamil, F. F. Basir, M. K. Syah, S. Maitra, C. C. Lam, N. S. Zainal, T. W. Hoong, A. B. Muhamad, M. B. Mohammad, 2021, Step change in reservoir imaging through massive gas cloud using rich azimuth ocean bottom nodes, Time-lag full waveform inversion and Q reverse time migration: IPTC 2021, accepted for publication.

Wang, P., Z. Zhang, Z. Wei, and R. Huang, 2018, A demigration-based reflection full-waveform inversion workflow: 88th Annual International Meeting, SEG, Expanded Abstracts, 1138–1142, doi: https://doi.org/10.1190/segam2018-2997404.1.

Xu, S., D. Wang, F. Chen, Y. Zhang, and G. Lambaré, 2012, Full waveform inversion for reflected seismic data: 74th Conference and Exhibition, EAGE, Extended Abstracts, W024, doi: https://doi.org/10.3997/2214-4609.20148725.

Yusoff, Y. B. M., N. A. M. Radzi, A. Khalil, and A. Amdan, 2015, Reservoir characterization using 3D 4C OBC seismic dataset in Sepat Field, Malay Basin, a first in PCSB: Seismic Driven Reservoir Characterization and Production Management Symposium, EAGE, Extended Abstracts, 25599, doi: https://doi.org/10.3997/2214-4609.201412311.

Zhang, Z., J. Mei, F. Lin, R. Huang, and P. Wang, 2018, Correcting for salt misinterpretation with full-waveform inversion: 88th Annual International Meeting, SEG, Expanded Abstracts, 1143–1147, doi: https://doi.org/10.1190/segam2018-2997711.1.